Electronic Supplementary Information

Tetradecahedral Cu@Ag Core-Shell Powder with High Solid-State Dewetting and Oxidation Resistance for Low-temperature Conductive Paste

Yulian Zeng[a], Shuai Zou[a, b]*, Zhenzhen Chen[a], Zheng Lu[a], Mengfei Ni[a], Chen-Wei Peng[a], Zipeng Wang[a], Hua Sun[a], Xiaohong Zhang[b, c], Xiaodong Su[a]*

[a] School of Physical Science and Technology, and Jiangsu Key Laboratory of Thin Films, Soochow University, 1 Shizi Street, Suzhou 215006, China

[b] Jiangsu Key Laboratory of Advanced Negative Carbon Technologies, Soochow University, Suzhou, Jiangsu, China

[c] Institute of Functional Nano & Soft Materials (FUNSOM), Soochow University, Suzhou 215123, Jiangsu, China

*Corresponding authors. szou@suda.edu.cn (S. Zou); xdsu@suda.edu.cn (X. Su)

Experimental section

Cu@Ag powder was prepared from spherical Cu powder with particle sizes varying from 0.675 μm to 4.03 μm (Fig. S18), which was purchased from Guangzhou Metallurgical Group Co., Ltd. (Guangzhou, China). First, the oxide layer of the Cu powder (6.5 g) was ultrasonically removed in a mixed solution consisting of ammonium hydroxide (NH$_4$OH, Macklin, 25%–28%, 7.125 mL·L^{-1}) and ammonium sulfate ((NH$_4$)$_2$SO$_4$, Sinopharm, 0.024 mol·L^{-1}), and then washed with deionized (DI) water three times.[1] After this pretreatment, a reducing solution containing glucose (C$_6$H$_{12}$O$_6$, Sinopharm, 0.278 mol·L^{-1}), sodium tartrate (C$_4$H$_4$O$_6$Na$_2$, Sinopharm, 0.052 mol·L^{-1}), polyethylene glycol 2000 (PEG, Macklin, 0.077 mol·L^{-1}), alkylphenol ethoxylates (OP-10, Macklin, 0.019 mol·L^{-1}), ethanol (Yonghua Chemical Co., Ltd, 80 ml·L^{-1}) and other additives was added to the Cu powder bath. The Ag

1

coating solution was then prepared. EDTA·2Na (Aladdin), thiourea (Aladdin, 0.6×10^{-5} mol) and silver nitrate ($AgNO_3$, Sinopharm, 0.055 mol) were dissolved in DI water (600 mL), and then TETA (Adamas) was instilled into the solution until the generated milky white sediment became colorless and transparent. After that, the Ag coating solution was dropped into the Cu powder bath under vigorous stirring and sonication via a syringe pump at room temperature. Finally, the prepared Cu@Ag powder was washed with DI water and ethanol, and then vacuum-dried at 60 °C.

The Tafel polarization curves were tested in complexing agent solutions using an electrochemical system (CHI660e) with a three-electrode configuration in which a Pt flake was used as the counter electrode, a Ag/AgCl electrode was used as the reference electrode, and a Ag flake was used as the working electrode. The composition of the complexing agent in the complexing agent solution corresponded to the plating solution of Sample F1 to Sample F6. Tafel polarization curves were obtained in the range of -1.5 V–1 V under a scan rate of 0.01 V/s. Before measurements, all specimens were immersed in the complexing agent solution until the open circuit corrosion potential reached equilibrium. The Tafel slope was calculated by $\eta = a + b\log(i)$, where η is the overpotential, i is the current density, a and b are the Tafel constant.

The surface morphology of the Cu@Ag powder was observed using field-emission scanning electron microscopy (FE-SEM) (S-4700, Hitachi) with energy-dispersive X-ray (EDX) and scanning transmission electron microscopy (STEM) (Talos F200X, FEI) at 200 kV. The particle size was measured with a laser particle analyzer (Mastersizer 3000). The crystal structures and oxidation of Cu@Ag powder and Cu powder were characterized by X-ray diffraction (XRD) (D8 Advance, Bruker) with Cu Kα ($\lambda = 0.15418$ nm). The long-term oxidation resistance of Cu@Ag powder was analyzed by high-resolution transmission electron microscopy (HRTEM), EDX mapping, and EDX line scanning (Talos F200X, FEI). The thermal stability of Cu powder and Cu@Ag powder in air was analyzed by thermogravimetric analysis (TGA) (TG/DTA7300, Hitachi) and differential scanning calorimetry (DSC) (YH-800B, Yuhong) in the temperature range of 30 to 700 °C under air at a heating rate of 10 °C·min^{-1}. The resistivity of the electrodes was tested with a four-point

probe (Keithley 2400). The damp heat (DH) tests were conducted in a constant-temperature and -humidity test chamber (Changzhou Mitutoyo Instrument Technology Co., Ltd.)

Supplementary Figures and Tables

Table S1 Literature overview of the research studies on the preparation of Cu@Ag powder by electroless plating.

References	The primary complexing agent	The secondary complexing agent and its role	Shape of Cu@Ag powder
2	Ammonium hydroxide	None	Irregular
1	Ammonium hydroxide	None	Spherical
3	Ammonium hydroxide	None	Irregular
4	Ammonium hydroxide	None	Flaky
5	Ammonium hydroxide	None	Spherical
6	Ammonium hydroxide	RE-608 copper-specific extractant (Chelating reagent of Cu^{2+} and prevented $[Cu(NH_3)_4]^{2+}$ from being formed and absorbed onto the surface of the copper powder.)	Irregular
7	Ammonium hydroxide	Ethylenediamine (Adjust pH)	Flaky
8	Ammonium hydroxide	None	Spherical
9	Ammonium hydroxide	None	Flaky
10	Ammonium hydroxide	None	Spherical
11	Ammonium hydroxide	None	Polyhedron with rough surface (Polyhedron Cu particles)
12	Ammonium hydroxide	None	Spherical and flaky
13	Ammonium hydroxide	None	Irregular
14	Ammonium hydroxide	None	Spherical and flaky
15	Ammonium hydroxide	None	Spherical and flaky

16	Ammonium hydroxide	None	Spherical
17	Ammonium hydroxide	None	Spherical
18	Triethylenetetramine/ diethylenetriamine/ Ethylenediamine/ Ethylenediamine/ Polyethylene polyamine/ Tetraethylenepentamine / Ammonium hydroxide	None	Unknown
19	Triethylenetetramine	None	Spherical
20	Triethylenetetramine	None	Spherical
21	EDTA·4Na	Ammonium carbonate (Adjust pH)	Unknown
22	EDTA	None	Spherical
23	EDTA	None	Spherical and flaky
24	Sodium citrate	None	Irregular
25	Thiosemicarbazide	None	Rough nanopolyhedra

Table S2 Stability constants of Cu^{2+} and Ag^+ with different complexing agents.

	Ammonium hydroxide	EDTA	TETA
Cu^{2+}	13 [26]	18.8 [27]	20.4 [28]
Ag^+	7.2 [29]	7.32 [29]	7.7 [30]
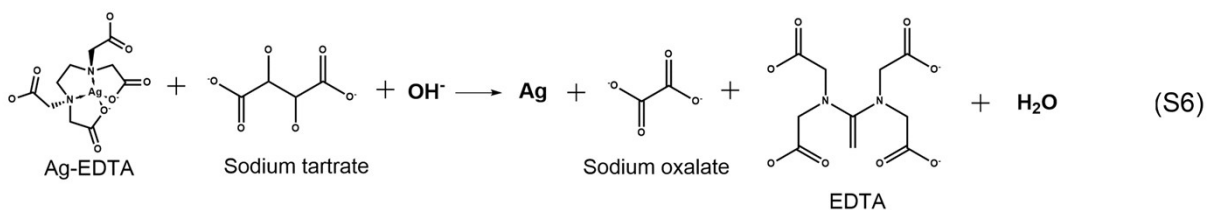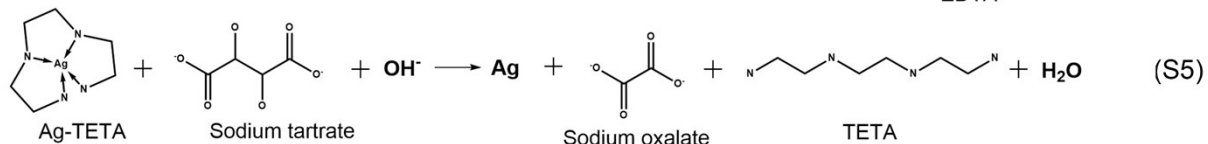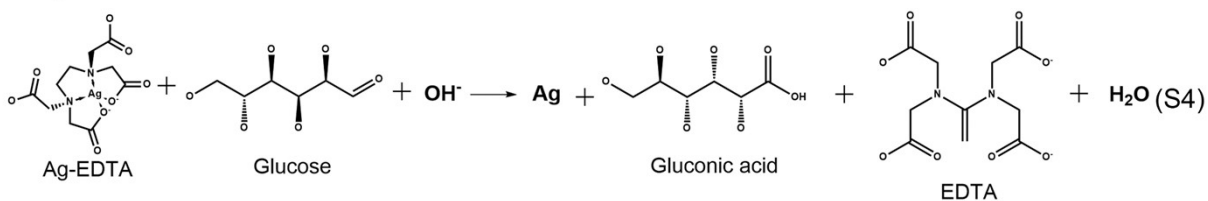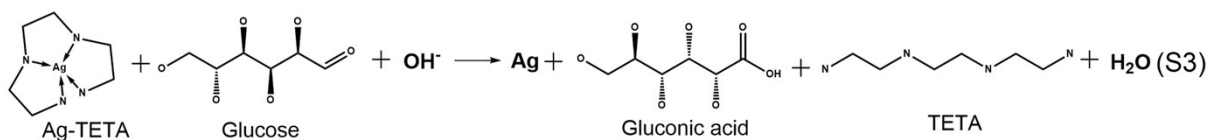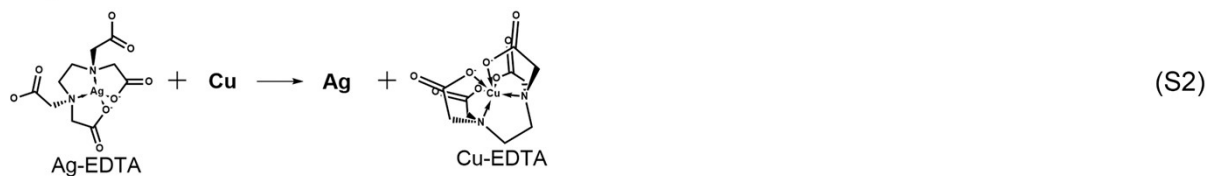
Fig. S1 Reaction equations of Ag shell growth.
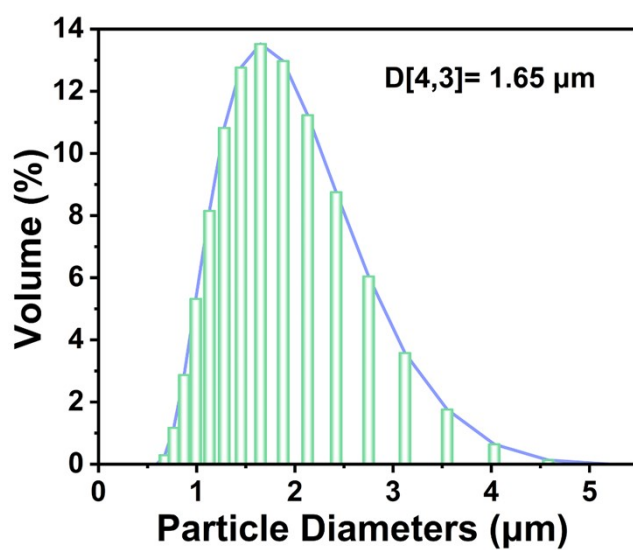
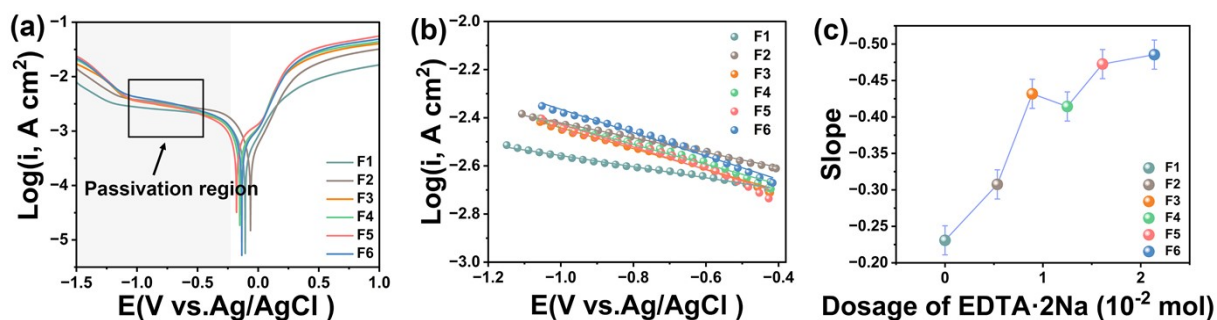**Fig. S2** Particle size distribution of tetradecahedral Cu@Ag powder.

Fig. S3 (a) Tafel polarization curves of Ag flakes tested in complexing agent solutions with different compositions. (b) Tafel plots derived from the passivation region marked by the black box in (a) and their first-order fitting lines. (c) Calculated Tafel slopes of the curves corresponding to (b).
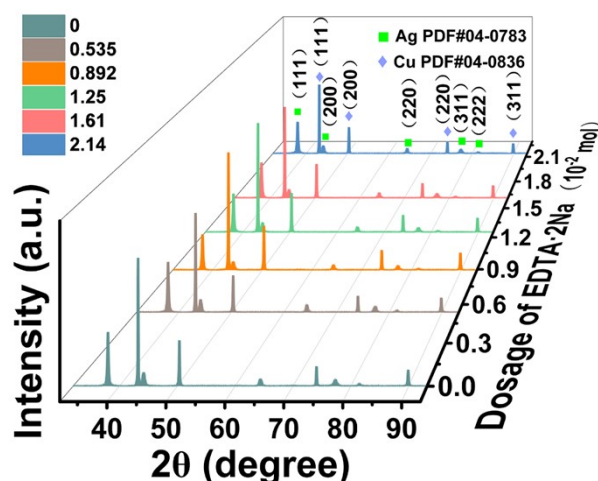

Fig. S4 XRD patterns of Cu@Ag powders prepared with different dosages of EDTA·2Na.

Detailed calculation data for the average grain size of the Ag shell:

Scherrer equation:

$$D = \frac{K\lambda}{\beta \cos\theta}$$

where D, K, λ, β, and θ are the grain size, geometric factor of spherical particles (0.89), wavelength of the radiation (0.15418 nm), full width at half maximum (FWHM) and Bragg angle, respectively.

Table S3 Average grain size of the Ag shell of Cu@Ag powder prepared with different dosages of EDTA·2Na at different dropping rates of the Ag coating solution.

Sample code	F1	F2	F3	F4	F5	F6	S1	S2
β [degree]	0.294	0.306	0.326	0.353	0.363	0.385	0.271	0.295
2θ [degree]	37.856	38.017	37.978	37.991	38.017	38.000	37.977	37.833
D [nm]	28.285	27.189	25.518	23.567	22.920	21.609	30.697	28.187
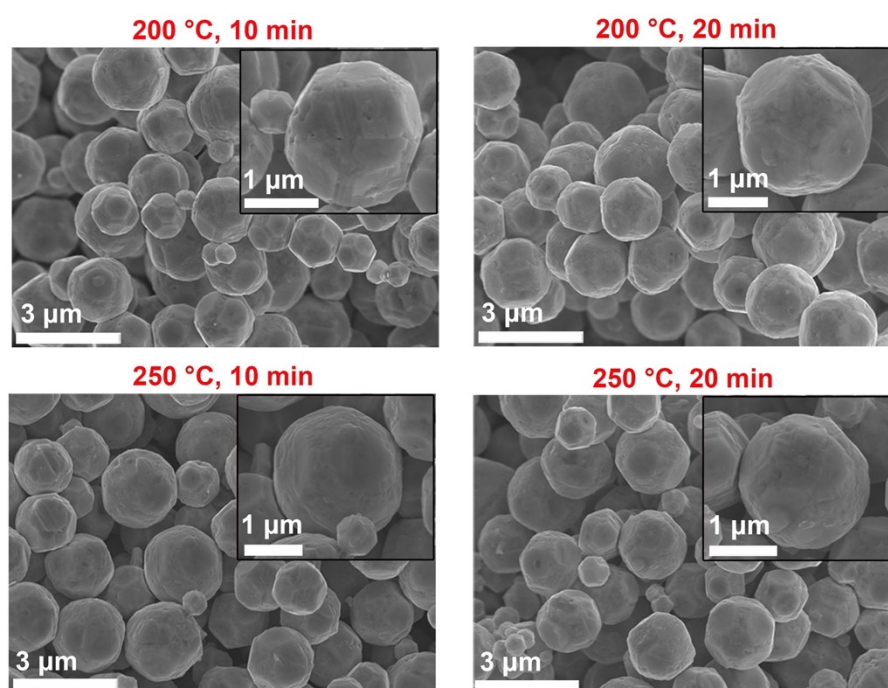
Fig. S5 SEM images of tetradecahedral Cu@Ag powder after heat treatment in air for 10 min (left) and 20 min (right) at 200 °C (top) and 250 °C (bottom).
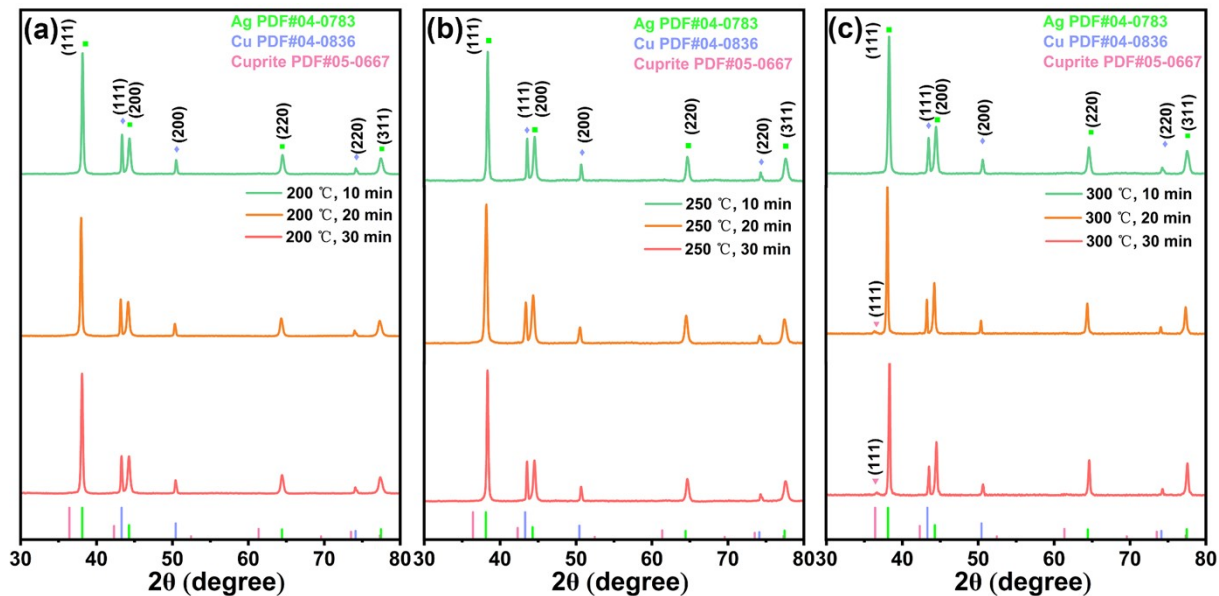
Fig. S6 XRD patterns of tetradecahedral Cu@Ag powder after heat treatment in air under different conditions: (a) at 200 °C for 10 min, 20 min, and 30 min; (b) at 250 °C for 10 min, 20 min, and 30 min; (c) at 300 °C for 10 min, 20 min, and 30 min.
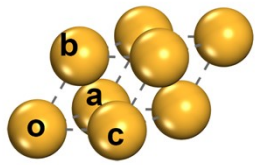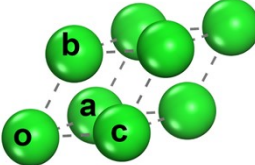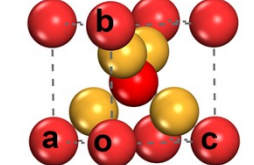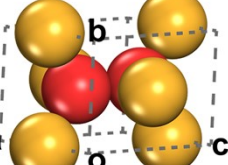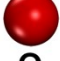
	Cu	Ag	Cu_2O	CuO
Cu ● Ag ● O ●	a=2.56062 Å b=2.56062Å c=2.56062Å	a=2.94195 Å b=2.94195 Å c=2.94195 Å	a=4.28781 Å b=4.28781 Å c=4.28781 Å	a=2.93890 Å b=2.93890 Å c=5.16072 Å

Fig. S7 Lattice constants and crystal structures of Cu, Ag, Cu_2O, and CuO.
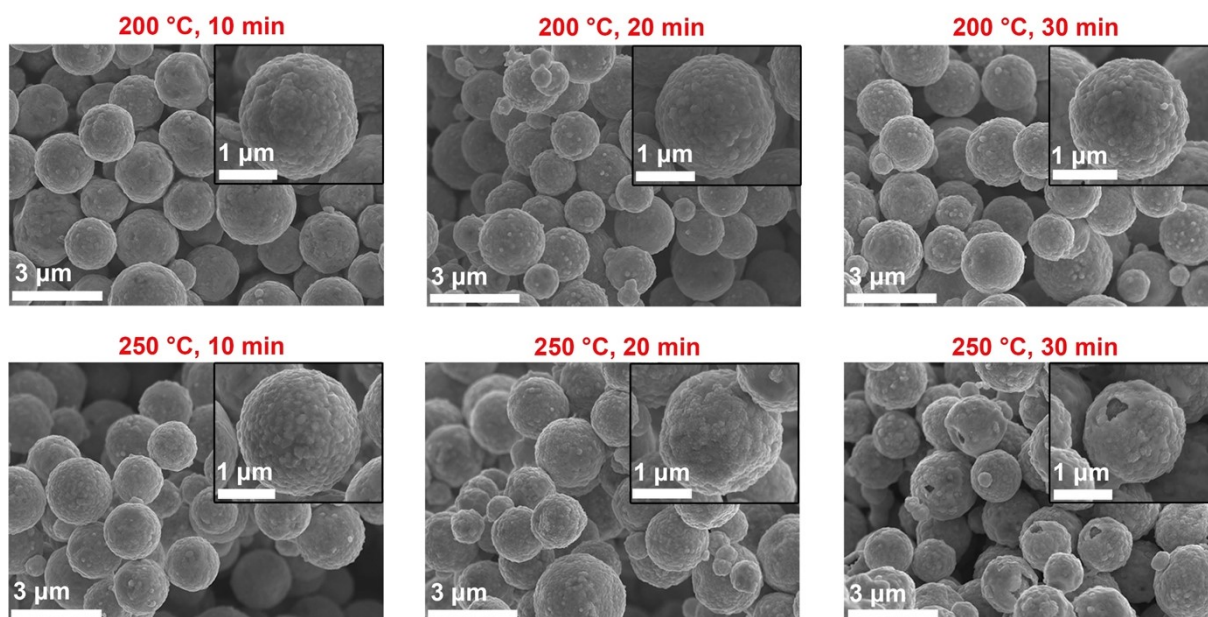
Fig. S8 SEM images of Sample F6 after heat treatment in air under different conditions: at 200 °C for 10 min, 20 min, 30 min (top); at 250 °C for 10 min, 20 min, 30 min (bottom).
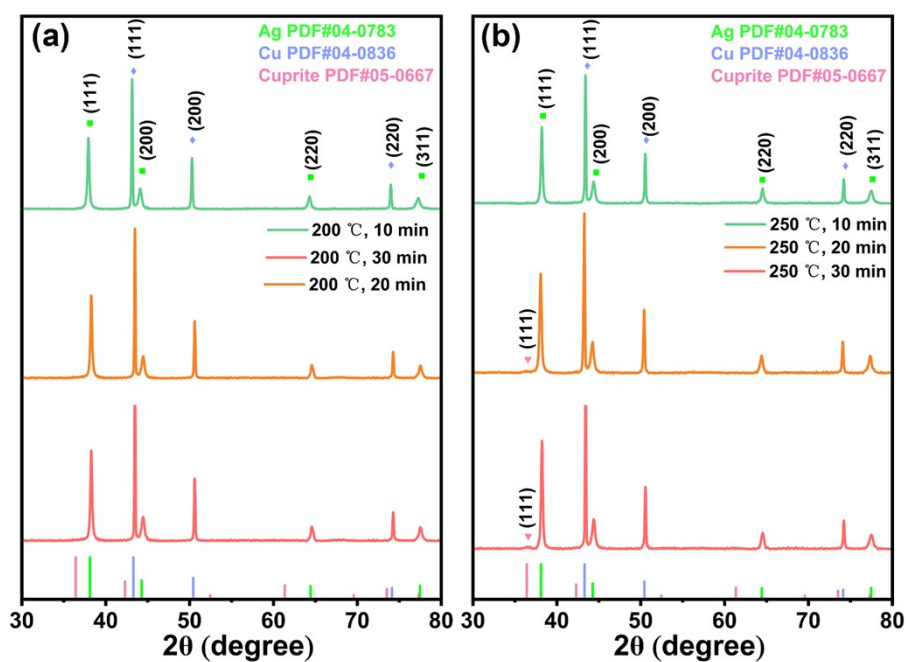

Fig. S9 XRD patterns of Sample F6 after heat treatment in air under different conditions: (a) at 200 °C for 10 min, 20 min, and 30 min; (b) 250 °C for 10 min, 20 min, and 30 min
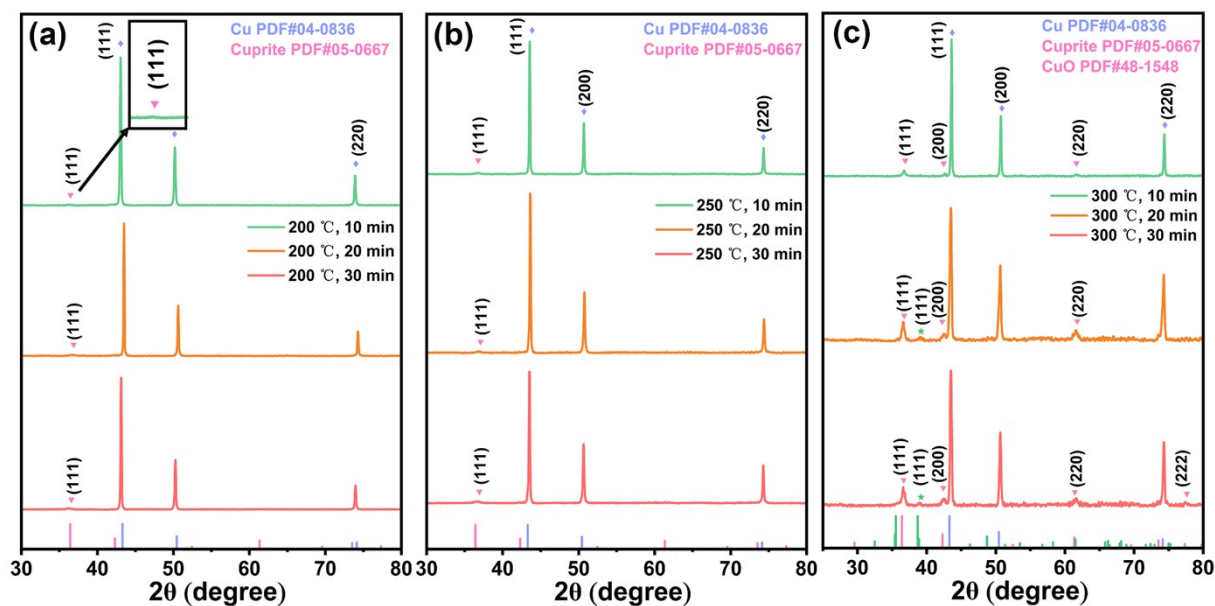
Fig. S10 XRD patterns of pure Cu powder after heat treatment in air under different conditions: (a) at 200 °C for 10 min, 20 min, and 30 min; (b) at 250 °C for 10 min, 20 min, and 30 min; (c) at 300 °C for 10 min, 20 min, and 30 min.
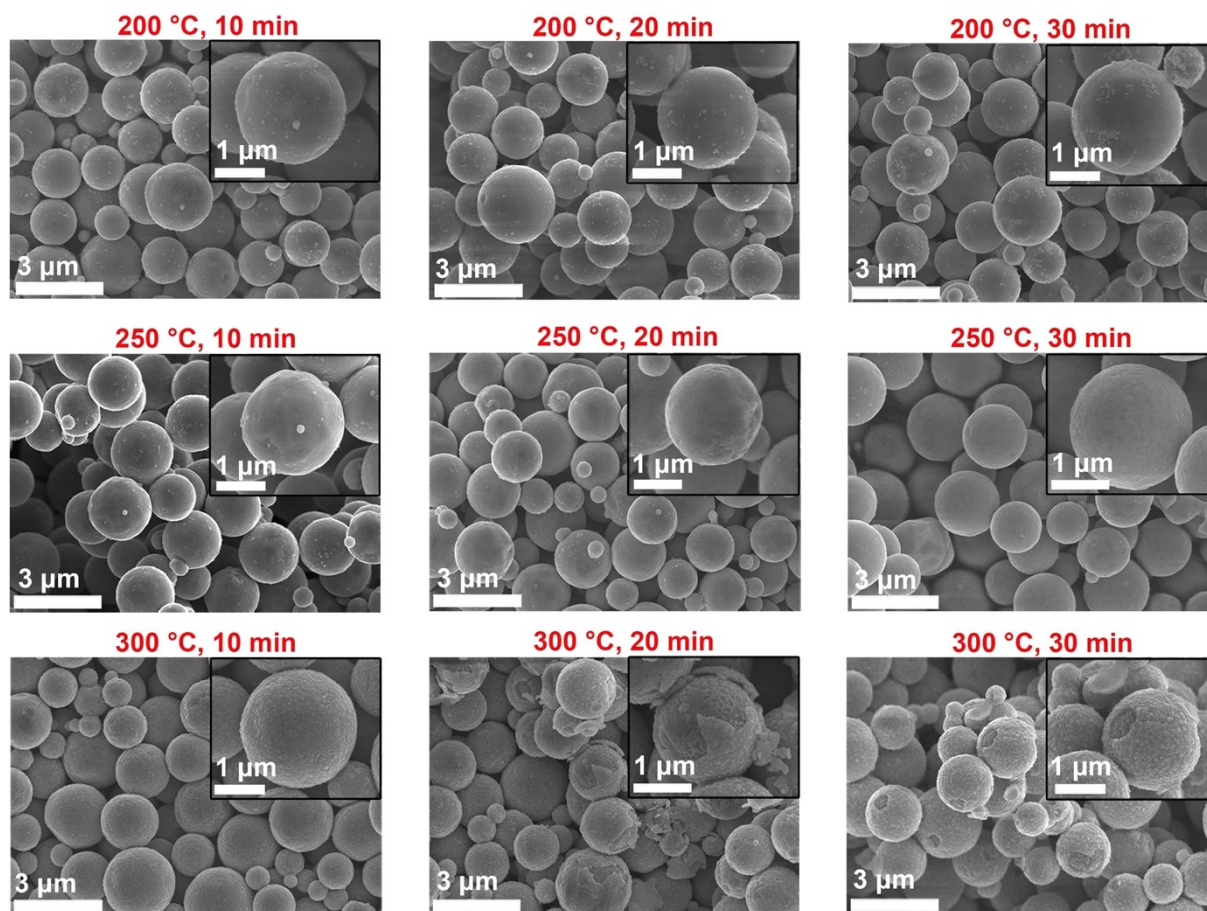

Fig. S11 SEM images of pure Cu powder after heat treatment in air under different conditions:

at 200 °C for 10 min, 20 min, and 30 min (top); at 250 °C for 10 min, 20 min, and 30 min (middle); at 300 °C for 10 min, 20 min, and 30 min (bottom).
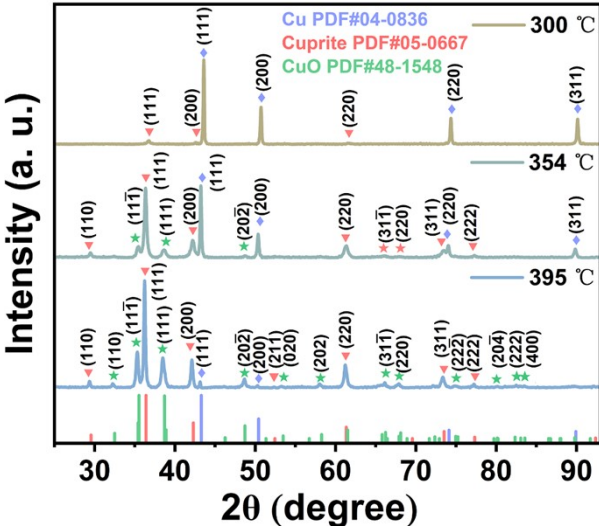

Fig. S12 XRD patterns of pure Cu powder after heat treatment in air for 10 min at 300 °C, 354 °C, and 395 °C.
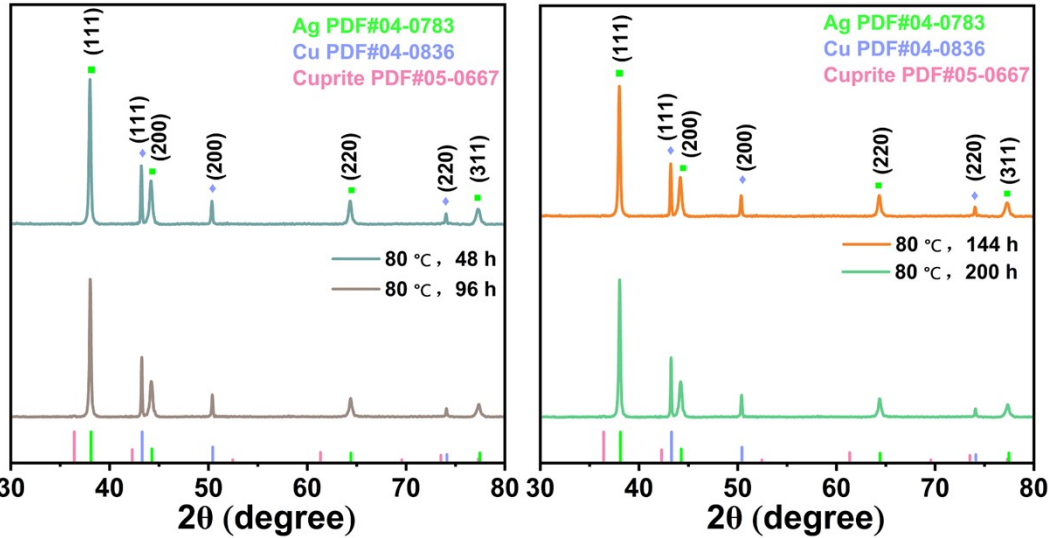
Fig. S13 Patterns of tetradecahedral Cu@Ag powder after the DH tests (+80 °C at 80% r.h.) for 200 h.
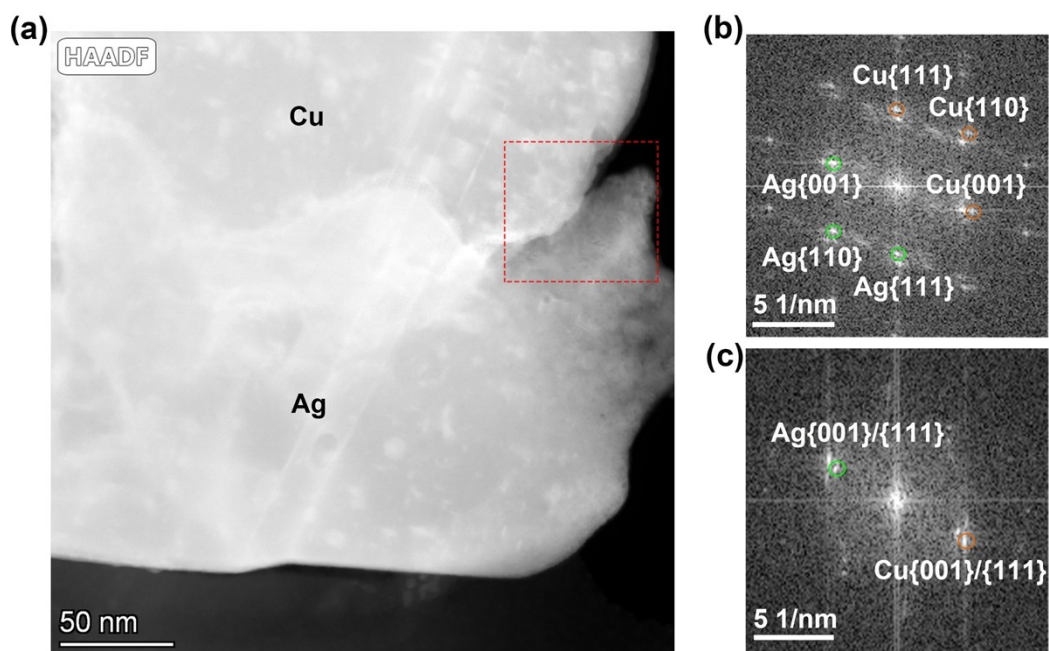
Fig. S14 (a) Partial cross-sectional low-magnification HAADF-STEM image of a tetradecahedral Cu@Ag particle after storage in air for 2 weeks. (b) FFT pattern corresponding to Fig. 4(g). (c) FFT pattern corresponding to Fig. 5(d).

Fig. S15 Photographs of Cu powder, tetradecahedral Cu@Ag powder (Sample S1), and spherical Cu@Ag powder (Sample S2).
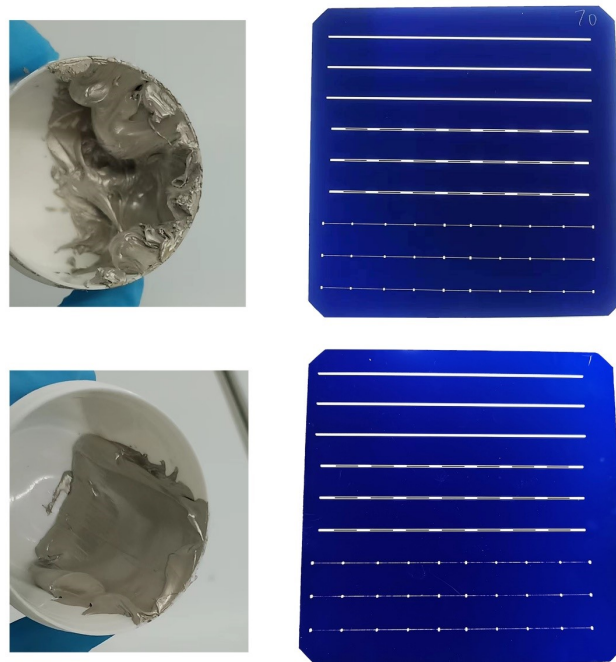
Fig. S16 Photographs of Paste S1 and Paste S2 (left) prepared with spherical Cu@Ag powder (top) and tetradecahedral Cu@Ag powder (bottom). The corresponding electrode pattern screen-printed on the SHJ substrates is shown on the right.

Simulation details of the bulk resistivity of stacked Cu@Ag particles

COMSOL 4.3 was used for this simulation work. The electrodes were constructed of a pair of Cu@Ag particles to simplify the calculation model. The Ag nanoparticles, resins, and air were used as background fillers. Fig. S17(a) shows the electrode model constructed by two spherical particles with point contacts (Model 1). The electric field diagram of applying a voltage of 1 V to both ends of the electrode is shown in Fig. S17(b). The current density distribution was calculated by the Poisson equation, and the input current was obtained by the current density integral. When the resistivity of the background fillers was set as half of the Ag shell, the resistivity of Model 1 was 7.19 μΩ·cm, which was close to the experimental value. Then, the electrode model constructed by two tetradecahedral particles with quadrilateral face contacts (Model 2) was established (Fig. S17c), and the resistivity of the background fillers adopted that of Model 1. A voltage of 1 V was also applied to the electrodes, and the resistivity of Model 2 was 5.31 μΩ·cm. In the same way, the resistivity of the electrode model constructed by two tetradecahedral particles with hexagonal face contacts
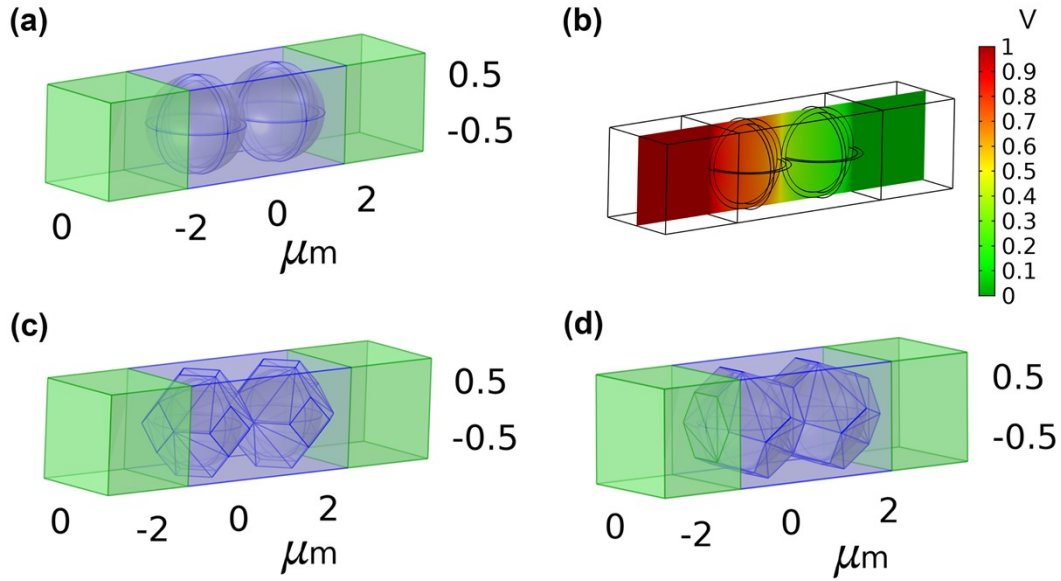
(Model 3) was 3.44 μΩ·cm (Fig. S17d).

Fig. S17 (a) Electrode model constructed by two spherical particles with point contacts (Model 1). (b) Electric field diagram of applying a voltage of 1 V to both ends of the electrode (Model 1). (c) Electrode model constructed by two tetradecahedral particles with quadrilateral face contacts (Model 2). (d) Electrode model constructed by two tetradecahedral particles with hexagonal face contacts (Model 3).

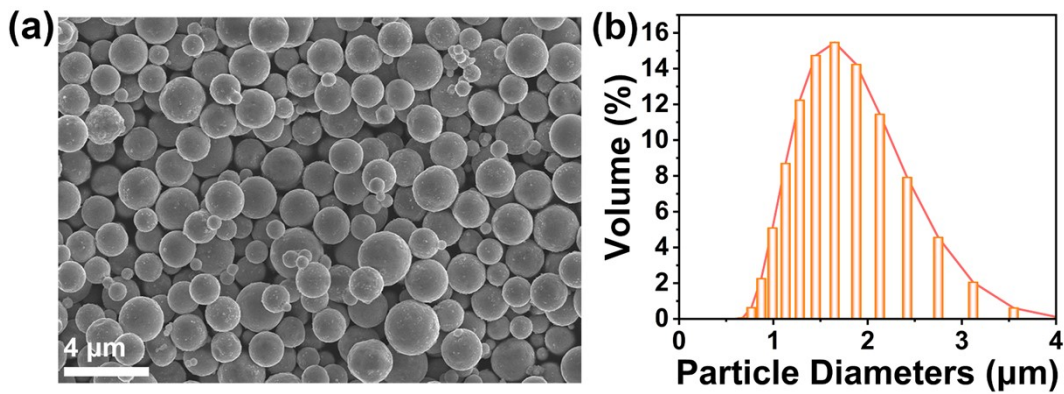**Fig. S18** (a) SEM image and (b) particle size distribution of raw Cu powder.

Notes and references

1   H. T. Hai, J. G. Ahn, D. J. Kim, J. R. Lee, H. S. Chung and C. O. Kim, *Surf. Coat. Tech.*, 2006, **201**, 3788-3792.
2   X. Xu, X. Luo, H. Zhuang, W. Li and B. Zhang, *Mater. Lett.*, 2003, **57**, 3987-3991.
3   B. Mei, Master dissertation, Huazhong University of Science and Technology, 2006. (In

Chinese)

4   J. J. Wu, X. Y. Zhu, Z. C. Zhu, F. Huang and G. M. Li, *Electronic Components & Materials*, 2006, **25**, 39-42. (In Chinese)

5   J. J. Kim, H. W. Lee, V. V. Dabhade, S. R. Kim, W. T. Kwon, D. J. Choi, H. Kim and Y. Kim, *Met. Mater. Int.*, 2010, **16**, 469-475.

6   X. G. Cao and H. Y. Zhang, *Powder Technol.*, 2012, **226**, 53-56.

7   H. P. Sun, K. J. Wang, X. L. Cai, G. Yue and Y. G. Chen, *Adv. Mater. Res.*, 2013, **750-752**, 1057-1062.

8   M. Wu, B. Lin, Y. Cao, J. Song, Y. Sun, H. Yang and X. Zhang, *J. Mater. Sci.-Mater. El.*, 2013, **24**, 4913-4918.

9   J. H. Kim and J.-H. Lee, *Korean J. Mater. Res.*, 2014, **24**, 617-624.

10 J. Shin, H. Kim, K. H. Song and J. Choe, *Chem. Lett.*, 2015, **44**, 1223-1225.

11 E. B. Choi and J.-H. Lee, *J. Alloy Compd.*, 2016, **689**, 952-958.

12 O. Güler, T. Varol, Ü. Alver and A. Çanakçı, *J. Alloy Compd.*, 2019, **782**, 679-688.

13 Y. L. Shi, Master dissertation, Southeast University, 2019. (In Chinese)

14 O. Güler, T. Varol, Ü. Alver and A. Canakci, *Mater. Today Commun*, 2020, **24**, 101153.

15 O. Güler, Ü. Alver and T. Varol, *J. Alloy Compd.*, 2020, **835**, 155278.

16 T. Varol, O. Güler, S. B. Akçay and H. C. Aksa, *Powder Technol.*, 2021, **384**, 236-246.

17 S. Djokic, M. Dubois and R. H Lepard, 1999, 5945158. (United States Patent)

18 F. B. Tan, Y. Z. Cai, L. Zhao and F. Z. Huang, *Precious Metal*, 2000, **21**, 8-11. (In Chinese)

19 J. Q. Hou, Master dissertation, Kunming University of Science and Technology, 2016. (In Chinese)

20 B. Wu, Master dissertation, Kunming University of Science and Technology, 2018. (In Chinese)

21 H. Kamiga, N. Nogami and A. Hirata, 2019, US 2019/0027620 A1. (United States Patent)

22 E. B. Choi and J.-H. Lee, *Appl. Surf. Sci.*, 2019, **480**, 839-845.

23 M. I. Kim, E. B. Choi and J.-H. Lee, *J. Mater. Res. Technol.*, 2020, **9**, 16006-16017.

24 Y.-h. Peng, C.-h. Yang, K.-t. Chen, S. R. Popuri, C.-H. Lee and B.-S. J. A. S. S. Tang, *Appl. Surf. Sci.*, 2012, **263**, 38-44.

25 X. B. Hu and L. Z. Hong, 2019, CN 110551995 B. (China Patent)

26 A. E. Martell and R. D. Hancock, *Metal complexes in aqueous solutions*, Springer Science & Business Media, 2013.

27 T. H. Madden, A. K. Datye, M. Fulton, M. R. Prairie, S. A. Majumdar and B. M. Stange, *Environ. Sci. Technol.*, 1997, **31**, 3475-3481.

28 L. Meier, *Clay. Clay Miner.*, 1999, **47**, 386-388.

29 W. G. Scribner and C. N. Reilley, *Anal. Chem.*, 1958, **30**, 1452-1462.

30 T. Saegusa, S. Kobayashi, K. Hayashi and A. Yamada, *Polym. J.*, 1978, **10**, 403-408.